Proceedings of the ASME 2021
Internal Combustion Engine Division Fall Technical Conference
ICEF2021
October 13-15, 2021, Virtual, Online

ICEF2021-67710

AMMONIA SLIP ESTIMATION BASED ON ASC CONTROL-ORIENTED MODELLING AND OBD NOX SENSOR CROSS-SENSITIVITY ANALYSIS

Pedro Piqueras, Benjamín Pla, Enrique José Sanchis, André Aronis

Universitat Politècnica de València, CMT-Motores Térmicos, Camino de Vera s/n, 46022 Valencia, Spain

ABSTRACT

The incoming emission regulations for internal combustion engines are gradually introducing new pollutant species, which requires greater complexity of the exhaust gas aftertreatment systems concerning layout, control and diagnostics. This is the case of ammonia, which is already regulated in heavy-duty vehicles and to be included in the emissions standards applied to passenger cars. The ammonia is injected into the exhaust gas through urea injections for NOx abatement in selective catalytic reduction (SCR) systems and can be also generated in other aftertreatment systems as three-way catalysts. However, ammonia slip may require removal on a dedicated catalyst called ammonia slip catalyst (ASC). The set consisting of the urea injection system, SCR and ASC requires control and on-board diagnostic tools to ensure high NOx conversion efficiency and minimization of the ammonia slip under real driving conditions. These tasks are based on the use of NOx sensors ZrO_2 pumping cell-based, which present as a drawback high cross-sensitivity to ammonia. Consequently, the presence of this species can affect the measurement of NOx and compromise SCR-ASC control strategies. In the present work, a methodology to predict ammonia and NOx tailpipe emissions is proposed. For this purpose, a control-oriented ASC model was developed to use its ammonia slip prediction to determine the cross-sensitivity correction of the NOx sensor placed downstream of the ASC. The model is based on a simplified solution of the transport equations of the species involved in the main ASC reactions. The ammonia slip model was calibrated using steady- and quasi-steady-state tests performed in a Euro 6c diesel engine. Finally, the performance of the proposed methodology to predict NOx and ammonia emissions was evaluated against experimental data corresponding to Worldwide harmonized Light vehicles Test Cycles (WLTC) applying different urea dosing strategies.

Keywords: Exhaust aftertreatment, Ammonia slip catalyst, NOx sensor, OBD.

NOMENCLATURE

ACRONIMS

ASC	Ammonia slip catalyst
ATS	Exhaust Aftertreatment Systems
DOC	Diesel oxidation catalyst
HP-EGR	High Pressure-Exhaust Gas Recirculation
OBD	On-board diagnostics
PGM	Platinum group metal
SCR	Selective catalytic reduction
SCRf	Selective catalytic reduction filter
WLTC	Worldwide harmonized Light vehicles Test Cycle
VGT	Variable geometry turbine

LATIN LETTERS

$A_{n,r}$	Preexponential factor
$Ea_{n,r}$	Activation energy
k_{cell}	Constant for cross-sensitivity
K_{CS}	Cross-sensitivity
$k_{n,r}$	Kinetic constant
k_T	Constant for temperature model
$\dot{m}$	Mass flow
M_n	Molecular weight
R_r	Reaction rate
T	Temperature
u	Gas velocity
x	Axial coordinate
X_n	Molar fraction

GREEK LETTERS

ε	Error
θ	Coverage
$\nu_{n,r}$	Stoichiometric constant
σ	Standard deviation
ψ	Maximum capacity

SUBCRIPTS

cell	Sensor cell
in	Inlet
out	Outlet
sensor	Sensor

SUPERSCRIPTS

t	Time

1. INTRODUCTION

The regulation of pollutant emissions in internal combustion engines has progressively restricted the emissions of nitrogen oxides (NOx) [1], which are harmful to human health and environment [2]. Despite the evolution of combustion strategies to reduce the NOx formation [3], the use of exhaust gas after-treatment systems (ATS) is required to meet the emission standards limits [4]. Among the available alternatives, the most widespread catalyst for NOx emission control in Compression Ignition engines is the selective catalytic reduction (SCR) system [5]. SCR systems are based on the reduction of NOx to N_2 by means of ammonia (NH_3) injected into the catalyst in the form of urea [6]. The SCR conversion efficiency depends on the amount of NH_3 loaded in the catalyst, which means that more ammonia is injected than necessary to reduce NOx [7], leading to a high NOx conversion efficiency, but consequently, more ammonia slip after the SCR catalyst. [8]. Moreover, the use of three-way catalysts in spark-ignition engines can lead to the formation of NH_3 [9]. To prevent tailpipe NH_3 emissions, ammonia slip catalysts (ASCs) are employed [10].

ASCs promote the oxidation of NH_3 in presence of O_2 to N_2 and water [11]. Currently, these systems combine an NH_3 oxidation catalyst component, commonly based on Platinum Group Metals (PGM), with an SCR catalyst since NOx species can be produced during the NH_3 oxidation [12]. There are several ways to combine these components. The most usual is to apply the SCR catalyst as a separate layer over the PGM one, thus creating a dual-layer washcoat structure. Nevertheless, the use of these two components together in a mono-layer structure can be also found in practical applications [13]. The reason for using two different substances is to achieve high NH_3 conversion efficiency increasing the selectivity of the oxidation to N_2 [14]. PGM particles are very active in the oxidation of NH_3 at the cost of low selectivity. This causes that at temperatures above 200 ºC the oxidation of NH_3 on Platinum produces significant amounts of NOx [13]. To improve the N_2 selectivity of the system, SCR catalyst impregnation is used, usually Cu or Fe zeolites [13], as a way to promote the final conversion of the NOx produced by the NH_3 oxidation mechanism with the entering NH_3 [15].

For the understanding, optimization and control strategies development of this type of systems, the use of computational models is of great interest. The mathematical solvers of such systems involve axial flow advection in the monolithic channels, as well as coupled reaction / diffusion processes in the catalytic layers [16]. In ASCs, the consideration of the NH_3 oxidation and NOx abatement reaction mechanism previously described is required [17].

The mathematical models that more accurately represent the real operation of this type of catalytic systems consist of non-linear partial differential equations in four independent variables, namely time and spatial coordinates. In this sense, it is possible to find models with different levels of complexity adapted to the particular application, from detailed design and analysis to on-board control. A simplification of this type of model is the one proposed by Torp *et al.* [13], based on a two-phase 1D-1D (pseudo 2D) single channel steady-state scheme for monolithic ASCs, distinguishing bulk gas from washcoat transport with up to two layers. Proposals of lower computational cost based on the use of reduced order models applied to two phase concepts are also available in the literature, such as the solution presented by Ratnakar *et al.* [18], based on multi-scale averaging method, or the Bisset's model [16], which provides an asymptotic solution of the reaction-diffusion problem. Finally, a step further in simplification consists of the use of pseudo-homogeneous models, which neglect the mass transfer from the bulk gas to the washcoat layers reducing the computational effort as compared to two-phase models [18].

In parallel, current and future regulations require the use of on-board diagnostics (OBD) to monitor the ATS performance and prevent its malfunction along lifetime [19]. Consequently, the control and diagnostics tasks of the SCR and ASC ideally require the use of NOx and also NH_3 sensors [20], the last still uncommon, combined to mathematical algorithms [21]. From the point of view of on-board measuring of both NOx and NH_3, the most common approach is the use of amperometric sensors based on ZrO_2 pumping cell [22]. This type of sensor presents NH_3 cross-sensitivity as main drawback, what means that the actual NOx emission may not correspond to the sensor signal due to the presence of NH_3 [23]. This correction of the cross-sensitivity may require the use of NH_3 sensors or multiple NOx sensors with different degrees of sensitivity to NH_3 [23] at the expense of higher cost.

In this context, the present work proposes a methodology to predict NH_3 and NOx exhaust tailpipe emissions. As a first step, a control-oriented ASC model was developed to provide a prediction of the NH_3 slip at the ASC outlet using as input NOx and NH_3 emissions downstream the SCR system. This NH_3 prediction was used to determine the cross-sensitivity correction of the NOx sensor placed downstream of the ASC. The ASC model is based on a simplified solution of the transport equations of the reactants governing the main paths of the ASC reaction mechanism. The quasi-steady one-dimensional species conservation equation is explicitly solved under the assumption of negligible diffusion limitations, i.e. pseudo-homogeneous approach [18], and non-competitive reactions. It keeps the fundamental physical and chemical nature of the actual process while providing low complexity and computational effort

required for efficient OBD. The combined prediction of tailpipe NH_3 and NOx emissions was evaluated on a Euro 6 diesel engine installed on a fully instrumented test bench, a gas analyzer was also placed in the exhaust tailpipe to measure the actual emission of NH_3 and NOx separately. The performance of the proposed methodology was evaluated against experimental data corresponding to Worldwide harmonized Light vehicles Test Cycles (WLTC) tests in which different urea dosing strategies were imposed. As a result, the accuracy of the prediction of NH_3 and NOx tailpipe emissions is discussed, demonstrating the potential of modeling approaches to avoid the use of dedicated sensors for the NH_3 slip prediction, while improving the NOx measurement in the exhaust pipe.

2. MATERIALS AND METHODS

2.1 Experimental setup and test campaign

The engine used in this work was a serial production Euro 6c diesel engine for passenger car applications equipped with variable geometry turbine (VGT) and high-pressure exhaust gas recirculation (HP-EGR). Table 1 lists the main engine specifications.

TABLE 1: MAIN CHARACTERISTICS OF THE ENGINE.

Displaced volume	[cm3]	1499
Bore	[mm]	75
Stroke	[mm]	84.8
Number of cylinders	[-]	4
Compression ratio	[-]	16.4:1
Maximum torque	[Nm@rpm]	300@1750
Maximum power	[kW@rpm]	96@3750
Emission standard	[-]	Euro 6c
EATS	[-]	DOC+SCRf+ASC

This engine was installed on an engine test bench equipped with a Horiba DYNAS3 asynchronous dynamometer, allowing dynamic and steady-state tests. Moreover, to ensure that the model was capable to be used in a real-time application, it was implemented into Simulink environment, compiled by the dSpace system, and connect via an ETK-ECU interface to an open ECU as a way to imposed the urea injection rate. The engine aftertreatment system (EATS) consisted of a close-coupled DOC, SCRf and ASC. In particular, the ASC was a dual-layer washcoat flow-through monolithic catalyst whose main geometrical characteristics are shown in Table 2.

The exhaust line was instrumented with K-type thermocouples at the inlet and outlet of every ATS monolith and an Horiba FTIR MEXA-ONE-FT engine exhaust gas analyzer sampling pollutant emissions upstream and downstream of the ASC. Finally, a ZrO_2 pumping cell NOx sensor was placed at the ASC outlet.

This experimental setup was applied to perform a series of tests driven to provide controlled ASC boundaries for model calibration and validation. A series of steady-state operating conditions, quasi-steady mapping tests and WLTC were performed including variations in the urea dosing strategy to feed the ASC with different NH_3 concentration for the same fluid-dynamic conditions. To understand the application of each test, they are described in Sections 3.1 and 3.2, where the model performance is evaluated.

TABLE 2: ASC GEOMETRIC PARAMETERS.

Lenght	[m]	0.10
Diameter	[m]	0.14
Monolith Volume	[dm^3]	1.65
Channel cross-section	[-]	Square
Cell size	[mm]	0.9607
Wall thickness	[mm]	0.0762
Cell density	[cpsi]	600
Number of channels	[-]	15096
GSA (geometric specific area)	[1/m]	3574
CA (Catalytic area)	[m^2]	5.89

2.2 NOx & NH_3 estimation methodology

The proposed methodology to predict the NH_3 and NOx emissions downstream of the ASC is outlined in Figure 1. The NH_3 and NOx concentration, temperature and mass flow at the ASC inlet and a single NOx sensor located downstream of the ASC are considered as boundary conditions.

The use of two computational models is considered. The first model is a simplified ASC model that allows considering the NH_3 accumulation reactions, as well as the elimination of accumulated NH_3 through oxidation with O_2 in the PGM layer and with NOx in the SCR layer. The NH_3 oxidation mechanism using NOx is a simplified version of the complete SCR reactivity mechanism, considering that the set of reactions can be represented using the standard reaction of the SCR. Although it is assumed that this simplification allows a correct estimation of the NH_3 oxidation rate, it is considered that the lack of detail of the model makes it not suitable for the prediction of the NOx slip. For this reason, the focus of the ASC model is placed on the estimation of the NH_3 emission, being necessary the use of a NOx sensor to obtain the NOx emissions at the ASC outlet. To correct the effect of NH_3 emissions on the NOx sensor signal, a second model is used, which allows the cross-sensitivity estimation. This model makes it possible to use the NH_3 emissions estimated by the ASC model to reduce the error in the NOx emission measurement.

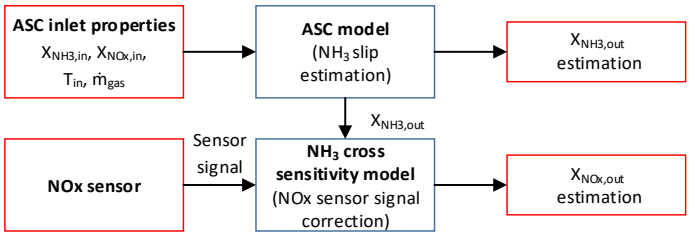

FIGURE 1: FLOW-CHART OF THE PROPOSED METHODOLOGY FOR ASC NH_3 AND NOx SLIP PREDICTION.

2.3 ASC model

The ASC model is based on a lumped approach solving the chemical species transport in discrete control volumes explicitly. In this work, the monolith was divided into two volumes, as sketched in Figure 2, which were governed by different characteristic reaction temperature.

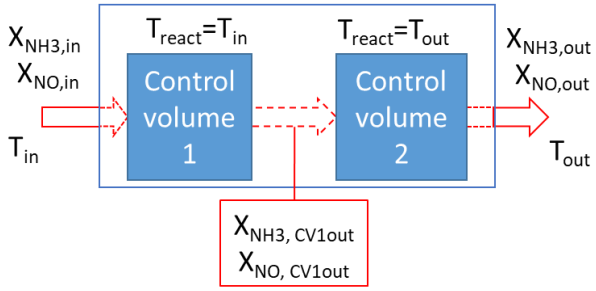

FIGURE 2: DISCRETIZATION OF THE ASC MODEL INTO CONTROL VOLUMES.

The temperature controlling the kinetics of the reaction mechanism in the first volume was assumed equal to the gas temperature provided by a sensor placed at the ASC inlet. The second control volume was aimed to represent the reactivity at the outlet region, so that the temperature of the gas at the ASC outlet was assumed. Since the engine did not account for an on-board temperature sensor at the ASC outlet, this temperature was calibrated from test bench temperature measurements correlating with the ASC gas inlet temperature on-board measurement according to Equation 1 [24].

$$T_{out}^{t} = k_{T,1} T_{out}^{t-1} + \left(1 - k_{T,1}\right) T_{in}^{t} + k_{T,2} \quad (1)$$

Due to the low amount of energy released by the reactions that take place in the ASC [25], this heat transfer model was decoupled from the chemical reactivity model. Nevertheless, its calibration, which was based on engine tests with urea injection, accounts implicitly for the energy released by the reactions.

In each control volume, the ASC model computed the variation in NH_3 and NOx along every control volume caused by the physisorption of NH_3 on the zeolites composing the SCR layer, the NOx reduction as well as the NH_3 oxidation to N_2 and NO. Equations 2-5 show the specific reactions considered in the model. This set of reactions is a reduced proposal of the global mechanism of an ASC [15], highlighting the fact that only the standard reaction of the SCR was considered. On the one hand, this assumption responds to the need of NH_3 slip estimation with low computational effort. On the other hand, the NO_2 concentration at the ASC inlet is several orders of magnitude lower than that of NO [23]. The NO_2 estimation would require additional model features concerning combustion conditions as well as the transport of NO_2 along the catalyst, unbalancing the computational effort to accuracy trade-off negatively.

$$NH_3 + Zeol \rightleftharpoons NH_3 \bullet Zeol \ \text{(R1,R2)} \quad (2)$$

$$NH_3 \bullet Zeol + \frac{3}{4} O_2 \rightarrow \frac{1}{2} N_2 + \frac{3}{2} H_2O \ \text{(R3)} \quad (3)$$

$$NH_3 \bullet Zeol + \frac{5}{4} O_2 \rightarrow NO + \frac{3}{2} H_2O \ \text{(R4)} \quad (4)$$

$$NH_3 \bullet Zeol + NO + \frac{1}{4} O_2 \rightarrow N_2 + \frac{3}{2} H_2O \ \text{(R5)} \quad (5)$$

The NO and NH_3 conversion efficiency were determined solving the one-dimensional chemical species transport [26] assuming quasi-steady flow and neglecting the mass transfer from the bulk gas and the washcoat according to the pseudo-homogeneous approach, so that:

$$u \frac{dX_n}{dx} = \sum \nu_{n,r} R_{n,r} \quad (6)$$

In Equation (6), $R_{n,r}$ and $\nu_{n,r}$ are the reaction rate and the stoichiometric coefficient of species *n* in reaction *r*. The reaction rate for every reaction was depending on the kinetic constant, which was modelled according to the Arrhenius equation, and the composition. The adsorption and desorption processes involving NH_3 and zeolite sites on the washcoat were modelled taking into the NH_3 gas concentration and the cumulative amount as a function of the surface coverage (θ_{NH3}) and the specific storage capacity of the washcoat (ψ_{NH3}):

$$R_{R1} = k_{NH_3,R1} \psi_{NH_3} \left(1 - \theta_{NH_3}\right) X_{NH_3} \quad (7)$$

$$R_{R2} = k_{NH_3,R2} \psi_{NH_3} \theta_{NH_3} \quad (8)$$

The reaction rate of every NH_3 oxidation reaction (NOx reduction, NH_3 oxidation to N_2 and NH_3 oxidation to NO) was modelled as:

$$R_{R3} = k_{O_2,R3} \psi_{NH_3} \theta_{NH_3} \quad (9)$$

$$R_{R4} = k_{O_2,R4} \psi_{NH_3} \theta_{NH_3} \quad (10)$$

$$R_{R5} = k_{NOx,R5} \psi_{NH_3} \theta_{NH_3} X_{NOx,in} \quad (11)$$

Therefore, assuming no competitivity between reactions, the integration of Equation 6 yields the molar variation of the species *n* caused by the reaction *r* as:

$$u\frac{dX_{n,r}}{dx}=\nu_{n,r}R_{n,r}\rightarrow\int_{X_{n,in}}^{X_{n,in}+\Delta X_{n,r}}\frac{dX_{n,r}}{\nu_{n,r}R_{n,r}}=\int_{0}^{L}\frac{1}{u}dx \quad (12)$$

The concentration of NH_3 at the outlet of every control volume was calculated from the molar variation caused by the reactions involving NH_3 sorption in the washcoat as:

$$X_{NH_3,CVout}=X_{NH_3,CVin}+\Delta X_{NH_3,R1}+\Delta X_{NH_3,R2} \quad (13)$$

In a similar way, the cumulation of NH_3 in every control volume of the ASC was computed by means of the surface coverage as

$$\theta_{NH_3}^{\,t+1}=\frac{M_{NH_3}}{\overline{M}}\sum\Delta X_{NH_3s}\frac{\dot{m}}{\psi_{NH_3}}+\theta_{NH_3}^{\,t}, \quad (14)$$

where the variation in cumulated NH_3 was calculated from the transport of every reactant and the reaction mechanism stoichiometry as presented below:

$$\sum\Delta X_{NH_3s}=\frac{\nu_{NH_3s,R1}}{\nu_{NH_3,R1}}\Delta X_{NH_3,R1}+\frac{\nu_{NH_3s,R2}}{\nu_{NH_3,R2}}\Delta X_{NH_3,R2}+$$
$$\frac{\nu_{NH_3s,R3}}{\nu_{O_2,R3}}\Delta X_{O_2,R3}+\frac{\nu_{NH_3s,R4}}{\nu_{O_2,R4}}\Delta X_{O_2,R4}+\frac{\nu_{NH_3s,R5}}{\nu_{NOx,R5}}\Delta X_{NOx,R5}$$
$$=-\Delta X_{NH_3,R1}-\Delta X_{NH_3,R2}+\frac{4}{3}\Delta X_{O_2,R3}+\frac{2}{5}\Delta X_{O_2,R4}+\Delta X_{NOx,R5} \quad (15)$$

2.4 NH_3 cross-sensitivity for NOx sensor correction

The NH_3 cross-sensitivity model for the correction of the NOx sensor signal is described in detail by Pla *et al.* [23]. This model is based on the estimation of the oxidation rate of NH_3 to NOx within the sensor cell. This oxidation is highly dependent on the sensor cell temperature. Since this temperature cannot be measured, the energy balance in the sensor cell was solved assuming negligible cell volume, no heat transfer between the cell and the environment, constant electric heating rate and exothermics proportional to NH_3 molar fraction [23]. According to these hypotheses and rearranging the energy balance, the sensor cell temperature was finally expressed as

$$T_{cell}^{t+1}=T_{cell}^{t}+k_{cell,1}\left(T_{gas}^{t}-T_{cell}^{t}\right)+k_{cell,2}X_{NH_3}+k_{cell,3}, \quad (16)$$

where $k_{cell,i}$ are physically-based constants experimentally determined.

Once the cell temperature was determined an empirical correlation, based on error function (erf), was proposed to estimate de cross-sensitivity factor as [23]

$$K_{CS}^{t}=1+k_{cell,4}erf\left(\frac{T_{cell}^{t}-k_{cell,5}}{k_{cell,6}}\right), \quad (17)$$

therefore, NOx sensor signal can be expressed as the addition of the NOx concentration and the concentration of NH_3 times the cross-sensitivity factor:

$$X_{NOx,sensor}=X_{NOx,out}+K_{CS}^{t}X_{NH_3,out} \quad (18)$$

3. RESULTS AND DISCUSSION

3.1 ASC model calibration and validation

Figure 3 shows the calibration procedure of the ASC and NH_3 cross-sensitivity models. As a first step, the correlation of the temperature prediction at the ASC outlet was calibrated from the inlet gas temperature in a WLTC test in order to account for the more demanding dynamic conditions and a wide temperature range.

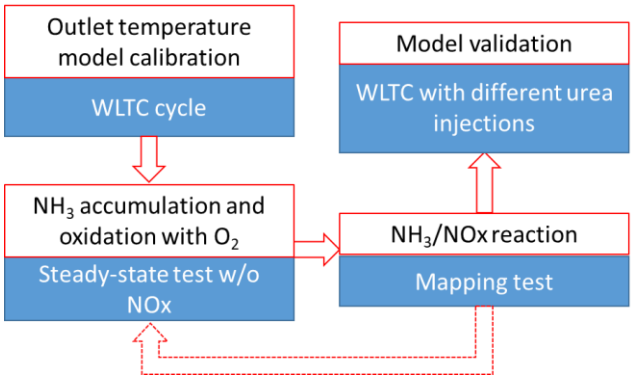

FIGURE 3: FLOW-CHART OF THE CALIBRATION AND VALIDATION PROCEDURE.

Figure 4(a) shows the calibration of the WLTC test, which provided the values for constants $k_{t,1}$ (0.817) and $k_{t,2}$ (-5.15). As observed, the model was able to capture with good accuracy the ASC outlet gas temperature, which in turn was applied as reaction temperature in the second control volume of the monolith. Figure 5 provides the error analysis of the ASC outlet gas temperature prediction based on the three-σ rule [27]. The three-σ rule defines three ranges around the mean value. The first one (1σ) considers the error threshold with a probability of 68.27% to be not exceeded assuming a normal distribution, i.e. 1σ represents the half-width interval of one standard deviation; the second range (2σ) accounts a probability of 95.45% and, finally, the 3σ error the 99.73% of points of the whole sample.

According to Figure 5, the error distribution underlines the low magnitude of the error in ASC outlet temperature calculation. The error was less than 10 °C for 1σ, while values within a half-width interval of two standard deviations (2σ) did

not exceed 20 °C. These low errors in calibration under dynamic operation were, in turn, kept in the prediction provided under different testing conditions, as shown in Figure 4(b), which presents the ASC outlet temperature along the quasi-steady state mapping test discussed next in this Section, and in Figure 4(c), which is dedicated to the steady-state operating points described in Table 3.

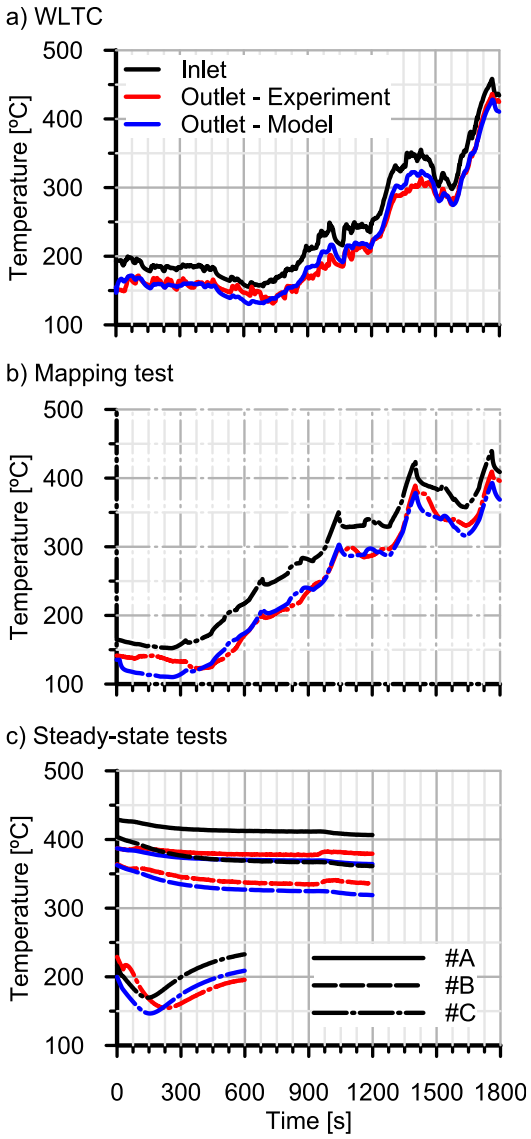

FIGURE 4: COMPARISON BETWEEN EXPERIMENTAL AND MODELED ASC OUTLET TEMPERATURE: (a) WLTC, (b) MAPPING TEST AND (c) STEADY-STATE TESTS.

The next step of the ASC model calibration was focused on the NH_3 adsorption-desorption and oxidation. Steady-state tests were performed to calibrate the kinetic term of the involved reactions. Table 3 lists the three operating points considered, which were monitored continuously to capture the dynamics in NH_3 slip imposed by the SCRf and the thermal transient. Every operating point covered a different temperature range, being modified the urea injection amount of the standard ECU strategy in order to feed the ASC with different NH_3 slips from the SCRf.

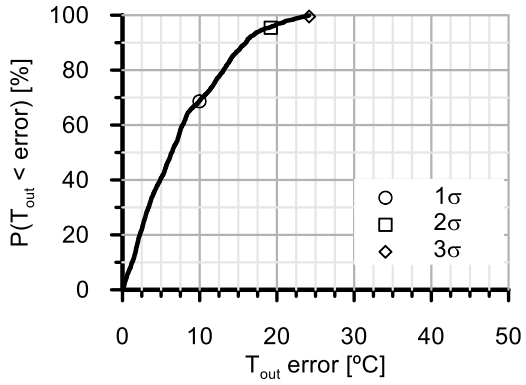

FIGURE 5: ASC OUTLET TEMPERATURE ERROR DISTRIBUTION IN WLTC TEST USED IN MODEL CALIBRATION.

TABLE 3: STEADY-STATE OPERATING POINTS FOR ASC MODEL CALIBRATION.

Point	Speed / torque	ASC T_{in}	Urea injection rate
#A	1750 rpm -150 Nm	~420ºC	150 mg/s (0-900 s) 250 mg/s (900 -1500 s)
#B	1750 rpm-114 Nm	~360ºC	150 mg/s (0-900 s) 250 mg/s (900 -1500 s)
#C	1750 rpm-56 Nm	~210ºC	100 mg/s (0-600 s)

Figure 6 shows the experimental NH_3 mass flow profiles at the inlet and outlet sections of the ASC comparing against the model prediction. As observed, once the SCRf NH_3 slip reached the ASC, a period of NH_3 cumulation within the ASC started without ASC NH_3 slip. This period was shorter as higher the inlet gas temperature (from plot (a) to (c)) because of the progressive weight of the desorption and oxidation rates, which moved the ASC balance towards the slip. In all cases, the model captured with good accuracy the slipped NH_3 mass flow, both in magnitude and dynamics. Only an advance in point #B slip prediction is remarkable (Figure 6(b)). In general terms, the model was very sensitive to the increase in urea injection, i.e. SCRf NH_3 slip, as observed in Figure 6(a) and (b), providing a very accurate prediction of the ASC NH_3 slip fashion.

Figure 7 summarizes the absolute NH_3 outlet mass flow error under these steady-state tests. The 1σ error was kept below 1.2 mg/s in all the tests. This threshold was kept even for 3σ band for point #A and increased just till 1.8 mg/s for point #B. The highest error was obtained at the lowest temperature (point #C), but still very low, ranging between 2.7 mg/s at 2σ and 3.1 mg/s in 3σ condition.

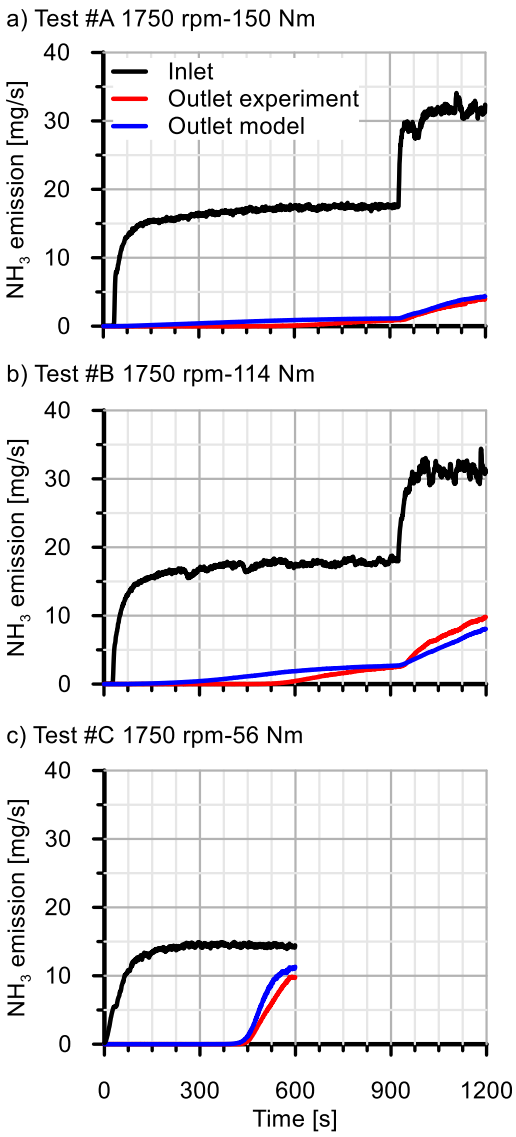

FIGURE 6: COMPARISON BETWEEN EXPERIMENTAL AND MODELED ASC NH3 SLIP UNDER DIFFERENT STEADY-STATE CONDITIONS WITH VARIABLE UREA INJECTION RATE.

Finally, the NOx reduction in the ASC model was calibrated assuming NO as representative species and the standard NO reaction, as described in Section 2.3. A mapping test was carried out in quasi-steady-state conditions to calibrate the NOx reduction while keeping the NH_3 cumulation and oxidation. This kind of test provided a wide sweep in exhaust gas mass flow, composition and temperature. Figure 8 represents the engine speed and torque profiles defining the test, as well as the ASC inlet temperature.

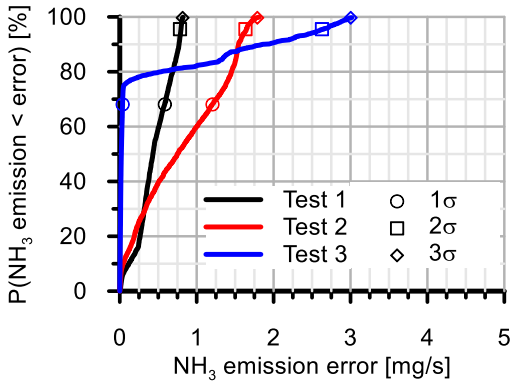

FIGURE 7: OUTLET NH_3 MASS FLOW ERROR DISTRIBUTION IN STEADY-STATE TESTS USED IN MODEL CALIBRATION.

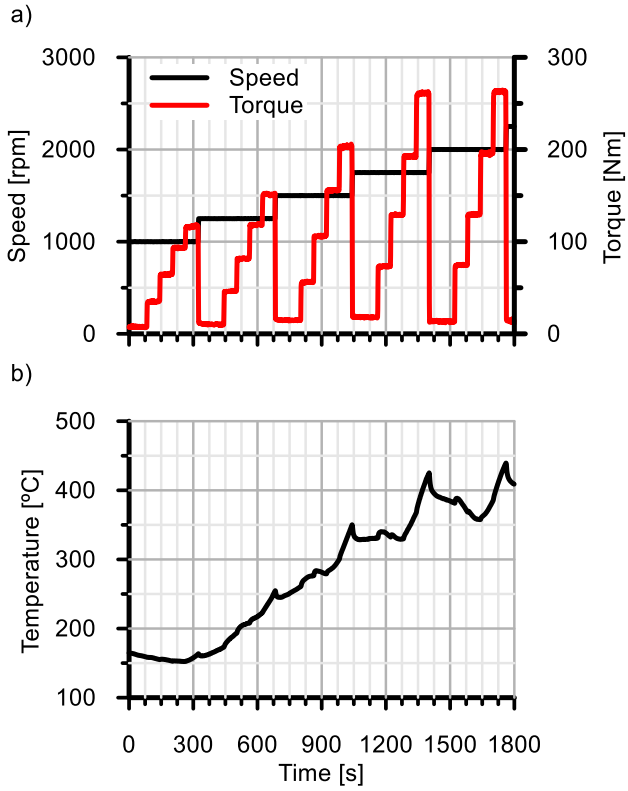

FIGURE 8: (a) SPEED AND TORQUE AND (b) ASC INLET GAS TEMPERATURE ALONG THE MAPPING TEST USED AS FINAL STEP OF THE ASC MODEL CALIBRATION PROCEDURE.

Figure 9 shows the comparison between experimental and modeled NH_3 and NOx emissions during the mapping test. The model showed good ability to predict the onset and magnitude of the NOx and NH_3 slips at the outlet of the ASC. Regarding the NH_3 mass flow, Figure 9(a) shows that the model reproduced the slip that occurred during the period from 900 to1300 s. On the other hand, Figure 9(b) also evidences the good sensitivity to the NOx slip, which was clear during the last phase of the lowest engine speed test (150-300 s) due to the lack of NH_3 in the

exhaust flow nor in the ASC (previous ASC NH_3 removal conditioning test). During the second and third engine speed tests a very slight NOx slip appeared at the highest engine load periods due to the residence time decrease. These slips were identified and well reproduced by the model. Finally, the model also captured the NOx slip peaks taking place during the final phase of the test (~1400 s) due to the high NH_3 oxidation rate at the corresponding high engine loads, in which the ASC inlet temperature ranged from 350 to 420 ºC, as shown in Figure 8(b).

According to the model trends in dynamic response shown in Figure 9, Figure 10 summarizes the model performance by means of the absolute error distribution in NOx and NH_3 tailpipe mass flows. As observed, the 1σ error was less than 0.5 mg/s both for NOx and NH_3. In the case of NH_3, which is the species of interest for on-board diagnostics proposals, the 2σ error was 0.75 mg/s and remained below 1.25 mg/s for 3σ. Regarding NOx, the error was slightly higher, reaching 1.75 mg/s for 2σ and 4 mg/s for the most limiting 3σ case.

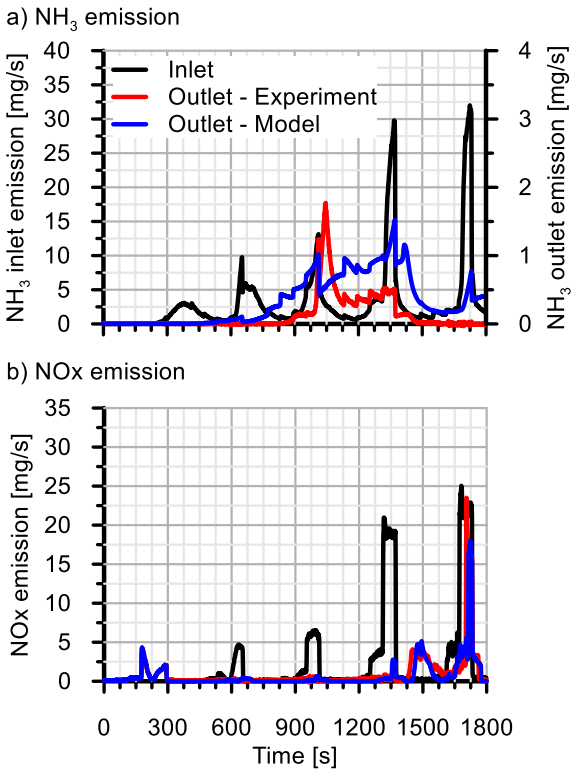

FIGURE 9: COMPARISON BETWEEN MEASURED AND MODELED NH_3 AND NOx EMISSIONS IN MAPPING TESTS.

As a closure of the calibration process, Table 4 shows the kinetic parameters corresponding to the proposed simplified ASC reaction mechanism, whose order of magnitude is in line with those found in the literature [25]. The model accuracy, keeping good response against transient excursions, confirms the potential of reduced order physical-based modelling approaches for control purposes.

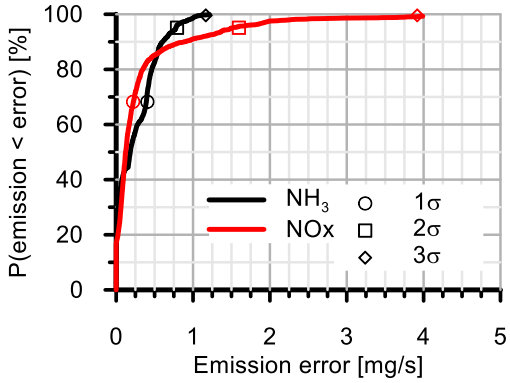

FIGURE 10: OUTLET NH3 AND NOx EMISSIONS ERROR IN MAPPING TEST.

TABLE 4: CALIBRATION OF THE ASC KINETIC PARAMETERS.

	A_n [-]	Ea [kJ/mol]
R1	7.4×10^4	0
R2	1.21×10^{10}	63.2
R3	3.07×10^8	65.7
R4	1.51×10^{12}	143.1
R5	2.59×10^5	31

From the calibration, two WLTC tests characterized by different urea injection strategies were used to validate the model prediction ability. In those tests, 1.2x and 1.5 x nominal urea injection were imposed as a way to provide more NH_3 to ASC across the WLTC cycle. The ASC inlet NH_3 mass flow and the resulting experimental and modeled NH_3 cumulative conversion efficiency are shown in Figure 11.

Figure 11 shows how the ASC exhibited a high NH_3 conversion efficiency in both WLTC tests. The low and medium WLTC velocity phases presented an experimental cumulative conversion efficiency higher than 97% for the case of 1.2x nominal injection and 98% for the 1.5x nominal injection strategy. In both cases, the model was close to 100% continuously. Because of the high efficiencies and the reduced NH_3 emission during these phases of the WLTC, the differences between the measured and modeled conversion efficiencies made no difference in the cumulative prediction of the NH_3 emissions at the ASC outlet. However, an increase in NH_3 emissions was observed along with a reduction of conversion efficiency during the high velocity and extra-high velocity phases. These results were produced by a combination of residence time reduction and temperature increase across the ASC. This reduction in conversion efficiency was correctly predicted by the model, being the differences between the cumulative experimental and modeled conversion efficiencies always lower than 2% in both WLTC tests. In this regard, the minimum NH_3 cumulative conversion efficiency achieved

during the extra-high velocity phases in the WLTC with 1.2x nominal injection was 97%, decreasing till 94.5% when the urea injection rate was increased a 50% with respect to the nominal one.

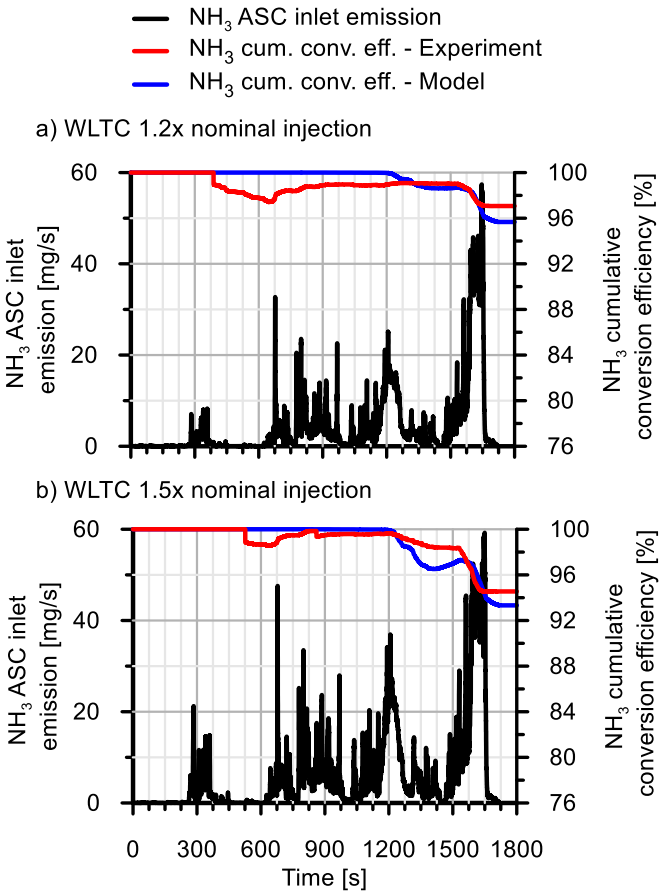

FIGURE 11: ASC INLET NH_3 EMISSION AND EXPERIMENTAL AND MODELED ASC NH_3 CONVERSION EFFICIENCY IN WLTC WITH (a) 1.2x NOMINAL UREA INJECTION AND (b) 1.5x NOMINAL UREA INJECTION.

3.2 APPLICATION OF CROSS-SENSITIVITY FOR NOx AND NH_3 ESTIMATION

WLTC tests were used to evaluate the interest of the cross-sensitivity correction of the NOx sensor from the NH_3 prediction. The actual NOx emission measurement was provided by Horiba MEXA-ONE-FT, whose results were compared with those obtained by the NOx sensor and when applied the cross-sensitivity correction.

Figure 12 represents the NO_x emissions at the ASC inlet and the cumulative NOx conversion efficiency corresponding to WLTC tests increasing the nominal urea injection by 20% and 50%. In all cases, for the conversion efficiency calculation, the NOx emissions at the ASC inlet provided by the Horiba gas analyzer were used as a baseline. The results evidence that the NOx sensor measurement at the ASC outlet was able to capture the actual cumulative NOx conversion efficiency during the low and medium velocity phases. Along these phases there was not correction from the ASC model since the NH_3 conversion efficiency is 100% till 1200 s, as observed in Figure 11. The deviations in cumulative conversion efficiency between the Horiba MEXA measurement and the NOx sensor counterpart appeared along the high and extra-high velocity phases of the WLTC cycle. In fact, the onset of the decrease of the NOx sensor accuracy coincided with the NH_3 slip prediction from the ASC model (Figure 11). Therefore, the cross-sensitivity phenomenon led the NOx sensor to account for the slipped NH_3 emissions as NOx, making the NOx signal downstream of the ASC artificially high and reducing the conversion efficiency with respect to the actual one.

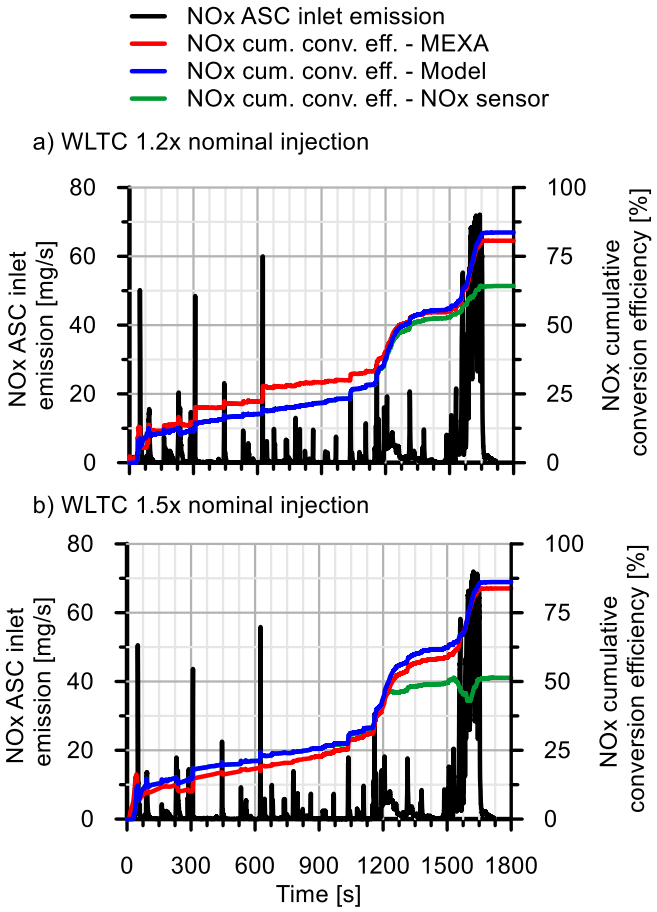

FIGURE 12: ASC INLET NOx EMISSIONS AND COMPARISON BETWEEN EXPERIMENTAL AND MODELED ASC NOx CONVERSION EFFICIENCY IN WLTC: (a) 1.2x NOMINAL UREA INJECTION AND (b) 1.5x NOMINAL UREA INJECTION.

The improvement in the prediction of the NOx emissions can be also computed in absolute error terms, as depicted in Figure 13, where both NH3 and NOx error distribution are shown. The results shown in Figure 13(a) are dedicated to the

WLTC tests corresponding to 1.2x nominal urea injection whilst Figure 13(b) corresponds to 1.5x nominal urea injection case. The accurate prediction in cumulative NH_3 conversion efficiency is also evidenced in absolute NH_3 emission at the ASC outlet, with errors below 1 mg/s and 2.5 mg/s for 2σ and 3σ respectively. Despite the similar capability to reproduce the cumulative NH_3 conversion efficiency (Figure 11), these absolute errors increased till 2.5 mg/s and 5 mg/s respectively when increasing the urea injection rate by a 50% with respect to the nominal calibration due to the higher NH_3 slip from the SCR during the low to high velocity phases.

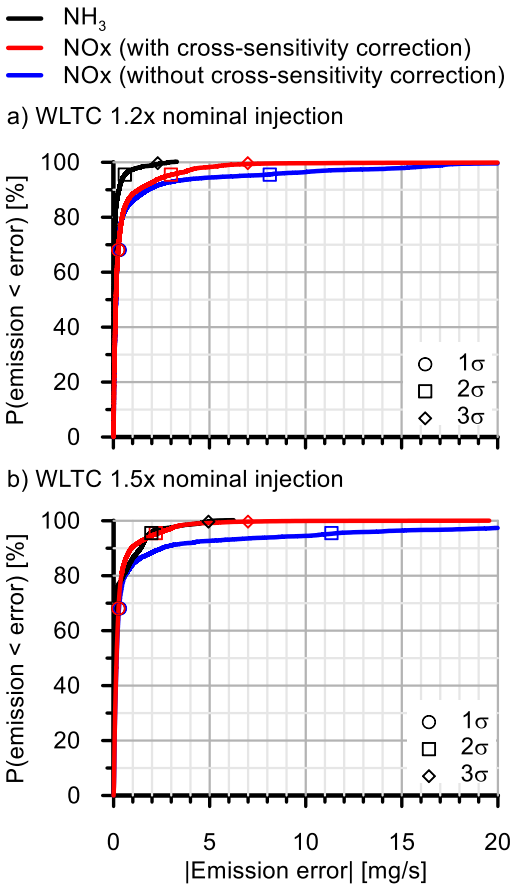

FIGURE 13: OUTLET NOx AND NH_3 MASS FLOW ABSOLUTE ERROR DISTRIBUTION IN WLTC WITH (a) 1.2x NOMINAL UREA INJECTION AND (b) 1.5x NOMINAL UREA INJECTION.

Nevertheless, this accuracy was high enough to bring a noticeable improvement of the NOx sensor accuracy. This is not observed in 1σ due to the lack of NH_3 emission and, hence, no sensor correction during most of the WLTC. However, the 2σ error was reduced from 8.5 mg/s in tailpipe NOx emission to 6 mg/s in 2σ and even 7 mg/s in 3σ after NH_3 cross-sensitivity correction in the WLTC test corresponding to 1.2x nominal urea injection. This higher accuracy was even more evident when applying the 1.5x nominal urea injection, providing the same absolute accuracy in NOx emission prediction after NH_3 cross-sensitivity correction than the 1.2x urea injection case despite the very high deviation of the direct NOx sensor measurement (2σ above 11 mg/s in NOx mass flow error).

Finally, Figure 14 shows the error distribution of the NH_3 mass flow predicted by the model, the direct NOx sensor signal and its counterpart when the cross-sensitivity correction is applied. The error distribution shows the model and sensor trends to overestimate or underestimate the emissions. In this sense, the NOx sensor error, without any kind of correction, showed a clear trend to overestimate the NOx emission due to NH_3 cross-sensitivity issues. In particular, the 2σ of the negative error was -0.7 mg/s while the positive counterpart increased till 8.4 mg/s for the case of the WLTC test corresponding to 1.2x nominal urea injection, which is shown in Figure 14(a). This is even more remarkable when increasing further the urea injection, as shown in Figure 14(b), where the 2σ of the negative error was reduced to -0.4 mg/s while the positive one increased to 11 mg/s. In view of these results, the NOx sensor overestimation makes difficult to use this signal for control and diagnostic tasks.

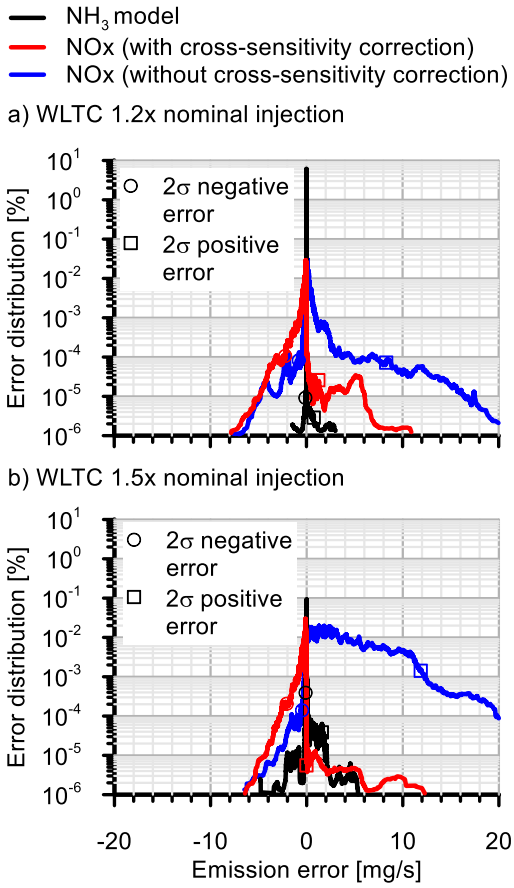

FIGURE 14: OUTLET NOx AND NH_3 MASS FLOW ERROR DISTRIBUTION IN WLTC WITH (a) 1.2x NOMINAL UREA INJECTION AND (b) 1.5x NOMINAL UREA INJECTION.

Moreover, the error distribution obtained for the model prediction of NH_3 during the WLTC test with 1.2x nominal urea provided a centered error distribution around 0 mg/s. As a result, the correction of cross-sensitivity on the NOx sensor signal, provided an almost centered error also for NOx. By contrast, the WLTC with 1.5x nominal urea injection showed a slight tendency to overestimate the emission of NH_3, being the positive 2σ error higher than the negative one. Consequently, the NH_3 overestimation led to the NOx underestimation after applying the cross-sensitivity correction.

4. CONCLUSIONS

This work has explored the combined use of control-oriented ASC modeling, based on simplified transport and reaction mechanism, and NOx sensor correction, based on cross-sensitivity determination, for the simultaneous prediction of NH_3 and NOx emissions at the ASC outlet. The NH_3 slip prediction from the ASC model, which neglects the reactivity limitations caused by bulk gas to washcoat mass transfer and competitivity between reactions, was used to correct the NOx sensor signal to consider the NH_3 cross-sensitivity. The reaction mechanism was also simplified assuming NH_3 oxidation to O_2 and NO as well as the NOx reduction, which was represented by the standard SCR reaction. Despite these modeling assumptions, the proposed approach reproduced the NH_3 and NOx slips in a wide variety of operating conditions following a calibration procedure that combined steady-state and quasi-steady-state engine operating conditions. The absolute ASC model error was less than 3 mg/s for a half-width interval equal to 2σ, properly predicting the NH_3 conversion efficiency.

The prediction abilities of the ASC and sensor models were checked against WLTC tests in which different urea dosing strategies were imposed, increasing the urea injection rate by up to 20% and 50% with respect to the nominal strategy. The results evidenced an accurate prediction of the NH_3 conversion efficiency along WLTC cycles with high sensitivity to the NH_3 concentration at the ASC inlet and to ASC NH_3 slip appearance at high vehicle velocities due to NH_3 residence time reduction. Complementary, the accurate NH_3 prediction with low computational effort enables the on-board NOx signal sensor correction to account for NH_3 cross-sensitivity without the need to add NH_3 sensors. The determination of the cross-sensitivity constant from the estimate of the sensor cell temperature provided a very accurate NOx conversion efficiency prediction in the ASC during low NH_3 slip conditions, i.e. almost negligible correction of the NOx sensor signal. In parallel, the NOx emission during the extra-high velocity WLTC phase was also captured despite the deviations in the original sensor signal providing an accurate NH_3 slip prediction both in magnitude and dynamic terms, i.e., with sensitivity to engine operating conditions and NH_3 concentration resulting from the specific urea injection strategy.

REFERENCES

[1] Ko, J., Jin, D., Jang, W., Myung, C. L., Kwon, S., Park, S. "Comparative investigation of NOx emission characteristics from a Euro 6-compliant diesel passenger car over the NEDC and WLTC at various ambient temperatures." *Applied energy* Vol. 187 (2017): pp. 652-662.

[2] Jonson, J. E., Borken-Kleefeld, J., Simpson, D., Nyíri, A., Posch, M., Heyes, C. "Impact of excess NOx emissions from diesel cars on air quality, public health and eutrophication in Europe." *Environmental Research Letters* Vol. 12 No. 9 (2017): pp. 094017.

[3] Jain, A., Singh, A. P., Agarwal, A. K. "Effect of split fuel injection and EGR on NOx and PM emission reduction in a low temperature combustion (LTC) mode diesel engine." *Energy* Vol. 122 (2017): pp. 249-264.

[4] Joshi, A. "Review of vehicle engine efficiency and emissions." *SAE International Journal of Advances and Current Practices in Mobility*. Vol. 2 (2020): pp. 2479-2507.

[5] Lisi, L., Cimino, S. "Poisoning of SCR Catalysts by Alkali and Alkaline Earth Metals." *Catalysts* Vol. 10 No. 12 (2020): pp. 1475.

[6] Shin, Y., Jung, Y., Cho, C. P., Pyo, Y. D., Jang, J., Kim, G., Kim, T. M. "NOx abatement and N2O formation over urea-SCR systems with zeolite supported Fe and Cu catalysts in a nonroad diesel engine." *Chemical Engineering Journal* Vol. 381 (2020): pp. 122751.

[7] Heywood, J. B. *Internal combustion engine fundamentals*. McGraw-Hill Education, New York (2008)

[8] Guardiola, C., Pla, B., Bares, P., Mora, J. "Model-based ammonia slip observation for SCR control and diagnosis." *IEEE/ASME Transactions on Mechatronics* Vol. 25 No. 3 (2020): pp. 1346-1353.

[9] DiGiulio, C. D., Pihl, J. A., Parks II, J. E., Amiridis, M. D., Toops, T. J. "Passive-ammonia selective catalytic reduction (SCR): Understanding NH3 formation over close-coupled three way catalysts (TWC)." *Catalysis Today* Vol. 231 (2014): pp. 33-45.

[10] Maunula, T., Tuikka, M., Wolff, T. "The Reactions and Role of Ammonia Slip Catalysts in Modern Urea-SCR Systems" *Emission Control Science and Technology* Vol. 6 No. 4 (2020): pp. 390-401.

[11] Ghosh, R. S., Le, T. T., Terlier, T., Rimer, J. D., Harold, M. P., Wang, D. "Enhanced Selective Oxidation of Ammonia in a Pt/Al2O3@ Cu/ZSM-5 Core–Shell Catalyst" *ACS Catalysis* Vol. 10 No. 6 (2020): pp. 3604-3617.

[12] Dhillon, P. S., Harold, M. P., Wang, D., Kumar, A., Joshi, S. Y. "Modeling and analysis of transport and reaction in washcoated monoliths: Cu-SSZ-13 SCR and dual-layer Cu-SSZ-13+Pt/Al2O3 ASC." *Reaction Chemistry & Engineering* Vol. 4 No. 6 (2020): pp. 1103-1115.

[13] Torp, T. K., Hansen, B. B., Vennestrøm, P. N., Janssens, T. V., Jensen, A. D. "Modeling and Optimization of Multi-functional Ammonia Slip Catalysts for Diesel Exhaust

Aftertreatment." *Emission Control Science and Technology* Vol. 7 (2021): pp. 7-25.
[14] Daya, R., Desai, C., Vernham, B. "Development and O2 Validation of a Two-Site Kinetic Model for NH 3-SCR over Cu-SSZ-13. Part 2. Full-Scale Model Validation, ASC Model Development, and SCR-ASC Model Application." *Emission Control Science and Technology* Vol. 4 No. 3 (2018): pp. 172-197.
[15] Sukumar, B., Dai, J., Johansson, A., Markatou, P., Ahmadinejad, M., Watling, T., Ranganath, B., Nande, A., Szailer, T. (2012). "Modeling of Dual Layer Ammonia Slip Catalysts (ASC)*." SAE 2012 World Congress & Exhibition*. Paper 2012-01-1294. Detroit, MI, April 24-26, 2012.
[16] Bissett, E. J. "An asymptotic solution for washcoat pore diffusion in catalytic monoliths*." Emission Control Science and Technology* Vol. 1 No. 1 (2015): pp. 3-16
[17] Scheuer, A., Votsmeier, M., Schuler, A., Gieshoff, J., Drochner, A., Vogel, H. "NH3-Slip Catalysts: Experiments Versus Mechanistic Modelling." *Topics in Catalysis* Vol. 52 (2009): pp. 1847-1851.
[18] Ratnakar, R. R., Dadi, R. K., Balakotaiah, V. "Multi-scale reduced order models for transient simulation of multi-layered monolith reactors." *Chemical Engineering* Vol. 352 (2018): pp. 293-305.
[19] Jiang, Y., Yang, J., Tan, Y., Yoon, S., Chang, H. L., Collins, J., Maldonado, H., Carlock, M., Clark, N., McKain, D., Cocker III, D., Karavalakis, G., Johnson, K. C., Durbin, T. D. "Evaluation of emissions benefits of OBD-based repairs for potential application in a heavy-duty vehicle Inspection and Maintenance program." *Atmospheric Environment* Vol. 247 (2021): pp. 118186.
[20] Brosha, E. L., Prikhodko, V. Y., Kreller, C. R., Pihl, J. A., Curran, S., Parks, J. E., Mukundan, R. "Response Characteristics of Stable Mixed-Potential NH 3 Sensors in Diesel Engine Exhaust." *Emission Control Science and Technology,* Vol. 3 No. 1 (2017): pp. 112-121.
[21] Bhardwaj, A., Bae, H., Namgung, Y., Lim, J., Song, S. J. "Influence of sintering temperature on the physical, electrochemical and sensing properties of α-Fe2O3-SnO2 nanocomposite sensing electrode for a mixed-potential type NOx sensor." *Ceramics International* Vol. 45 No. 2 (2019): pp. 2309-2318.
[22] Aliramezani, M., Ebrahimi, K., Koch, C. R., Hayes, R. E. "NOx sensor ammonia cross sensitivity analysis using a simplified physics based model" *Proceedings of Combustion Institute Canadian Section (CICS) Spring Technical Meeting University of Waterloo*, Montreal, QC, May 15-18, 2016.
[23] Pla, B., Piqueras, P., Bares, P., Aronis, A. "NOx sensor cross sensitivity model and simultaneous prediction of NOx and NH3 slip from automotive catalytic converters under real driving conditions." *International Journal of Engine Research* (2020). DOI 10.1177/1468087420966406.
[24] Guardiola, C., Dolz, V., Pla, B., Mora, J. "Fast estimation of diesel oxidation catalysts inlet gas temperature". *Control Engineering Practice* Vol 56 (2016) pp. 148-156.
[25] Nova, I., Tronconi, E. *Urea-SCR technology for deNOx after treatment of diesel exhausts*. Springer, New York (2014).
[26] Piqueras, P., García, A., Monsalve-Serrano, J., Ruiz, M. J. "Performance of a diesel oxidation catalyst under diesel-gasoline reactivity controlled compression ignition combustion conditions." *Energy conversion and management* Vol. 196 (2019): pp. 18-31.
[27] Gulati, S. T. "Cell Design for Ceramic Monoliths for Catalytic Converter Application" *1988 SAE International Fall Fuels and Lubricants Meeting and Exhibition*. Paper 881685. Portland, OR, October, 1988.